Supplementary Table 1

Cryo-EM data collection, refinement and validation statistics*

	300 mM K^+ (EMDB-24650) (PDB 7RR1)	3 mM K^+ (EMDB-24651) (PDB 7RR2)
Data collection and processing		
Magnification	130,000 x	130,000 x
Voltage (kV)	300	300
Electron exposure (e–/Å^2)	50	50
Defocus range (μm)	-0.6 to -2.5	-0.6 to -2.5
Pixel size (Å)	1.1	1.1
Symmetry imposed	C4	C4
Initial particle images (no.)		
Final particle images (no.)	232,371	358,026
Map resolution (Å)	3.4	3.1
FSC threshold	0.143	0.143
Map resolution range (Å)	3.2 – 6.6	2.9 – 5.5
Refinement		
Initial model used (PDB code)	5VA1	5VA1
Model resolution (Å)	3.6	3.2
FSC threshold	0.5	0.5
Model resolution range (Å)		
Map sharpening *B* factor (Å^2)	-111.0	-96.6
Model composition		
Non-hydrogen atoms	18548	18548
Protein residues	2324	2324
Ligands	0	0
B factors (Å^2)		
Protein	18.50	22.38
Ligand	n.a.	n.a.
R.m.s. deviations		
Bond lengths (Å)	0.004	0.004
Bond angles (°)	0.654	0.716
Validation		
MolProbity score	1.37	1.25
Clashscore	3.39	4.12
Poor rotamers (%)	0.20	0.00
Ramachandran plot		
Favored (%)	96.4	97.7
Allowed (%)	3.6	2.3
Disallowed (%)	0.0	0.0

Supplementary Figure 1

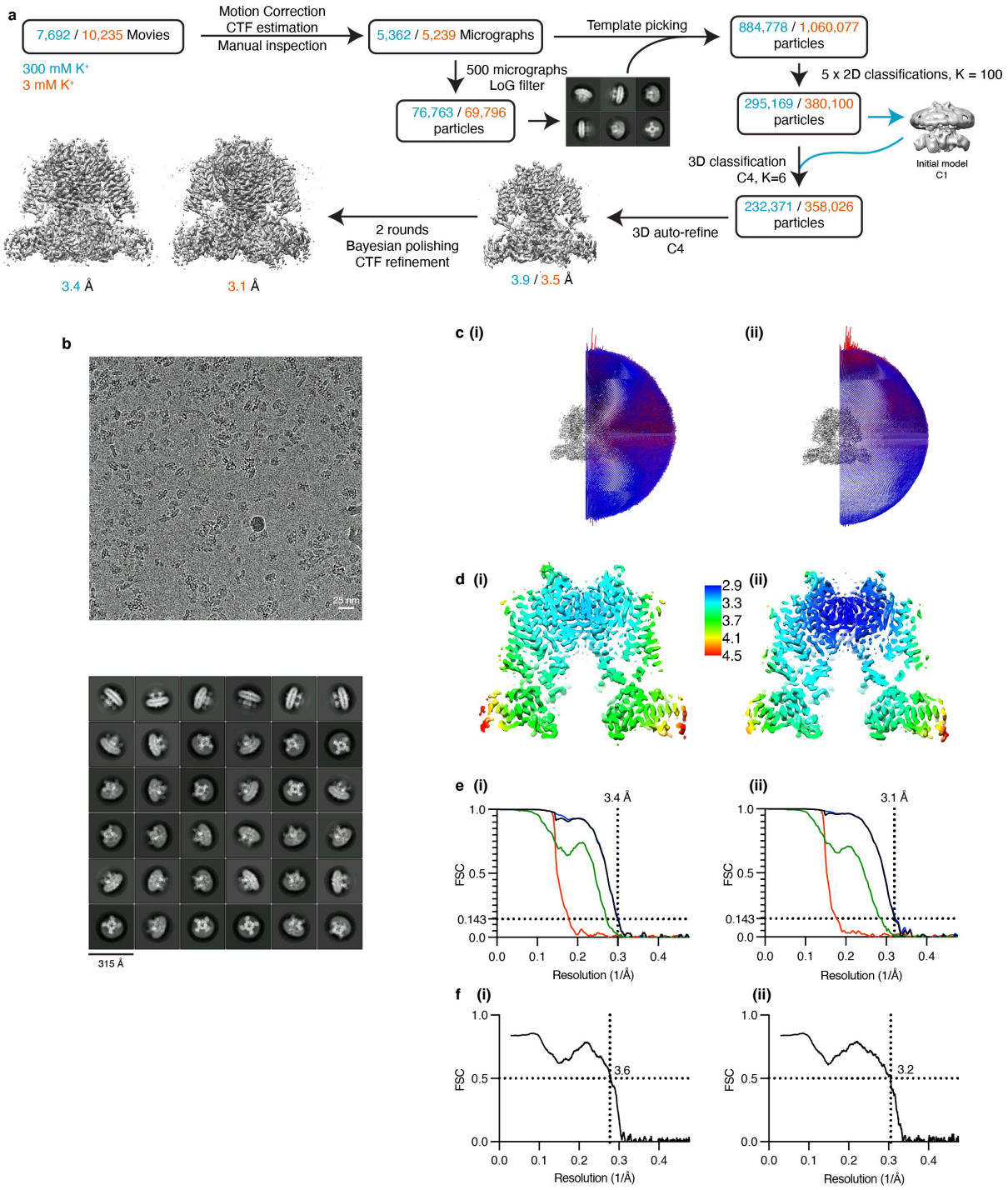

Supplementary Figure 1: **Summary for cryo-EM analysis of hERG Ts.**

(a) Flow chart of EM data processing for high [K^+] (cyan) and low [K^+] (orange) dataset. Details can be found in Methods section. (b) Representative electron micrograph and 2D class averages of hERG Ts for low [K^+] dataset. (c) Euler angle distribution of all particles used for final 3D reconstruction for (i) high [K^+] and (ii) low [K^+] dataset. (d) Local resolution projected on a centre cross-section of the final 3D reconstruction. (e) Gold-standard fourier shell correlation (FSC) curve for the 3D reconstruction. (f) FSC curves between atomic model and full map.

Supplementary Figure 2

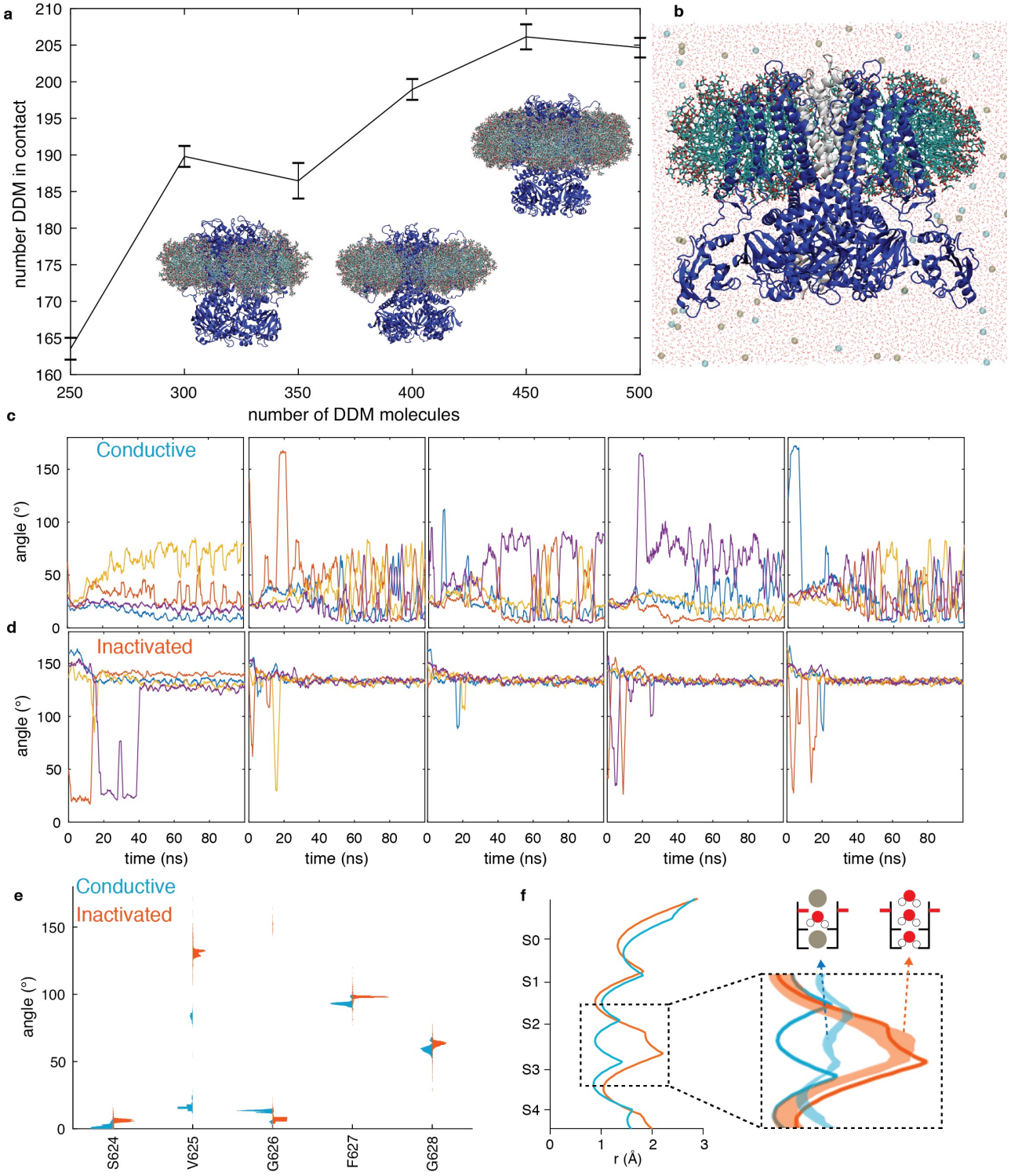

Supplementary Figure 2: MDFF fits to cryoEM maps for high and low K+ structures.

a. The optimal size of the micelle was determined by simulating HERG (PDB:5VA1) in 6 different sizes between 250 and 500 molecules of a simple pure detergent micelle (DDM). The number detergent molecules in contact with the protein is plateauing at 400-450 molecules showing that this is the optimal micelle size. **b.** Simulation system with the high K^+ HERG PDB structure

(Legend continued over page)

Supplementary Figure 2 continued

(shown in blue, with the TMD of the subunit at the front hidden and at the back in grey, for clarity) embedded in a micelle of 404 molecules consisting of detergent (DDM (300)), lipids (POPE (20), POPC (20), POPA (4)) and cholesterol derivative (cholesteryl hemisuccinate (60)) (shown as cyan (C), blue, (N), red (O) and olive (P) sticks) and surrounded by TIP3P water molecules[56] (shown as red sticks) and KCl (shown as olive and cyan spheres, respectively). **c,d.** Timeseries of the Val625 carbonyl angle for the five independent MDFF simulations for high K channel with ions in S2/S4 (c) and low K channel with an empty selectivity filter (d). For both systems, we see flipping and unflipping in the early part of the simulations. The high K channel converges to a mix of flipped and unflipped Val625 carbonyls, whereas in the low K channel all Val625 are flipped at the end of the simulations. **e.** Distribution plots of the angle of the backbone carbonyls in the selectivity filter for the high (blue) and low (orange) K^+ structures based on 250 energy minimised structures extracted from MDFF simulations. **f**. Plot of the selectivity filter radius for the high K (blue) and low K (orange) channel determined with HOLE[17]. Solid lines show the radius determined from the cryoEM fit and shaded area the radius determined for the 250 energy minimised structures extracted from MDFF simulations. The decreased radius in the MDFF simulations compared to the cryoEM fit at the Val625 carbonyls (between S2 and S3) in the high K channel arise comes from the Val625 carbonyl beings being in a mix of flipped and unflipped states.

Supplementary Figure 3

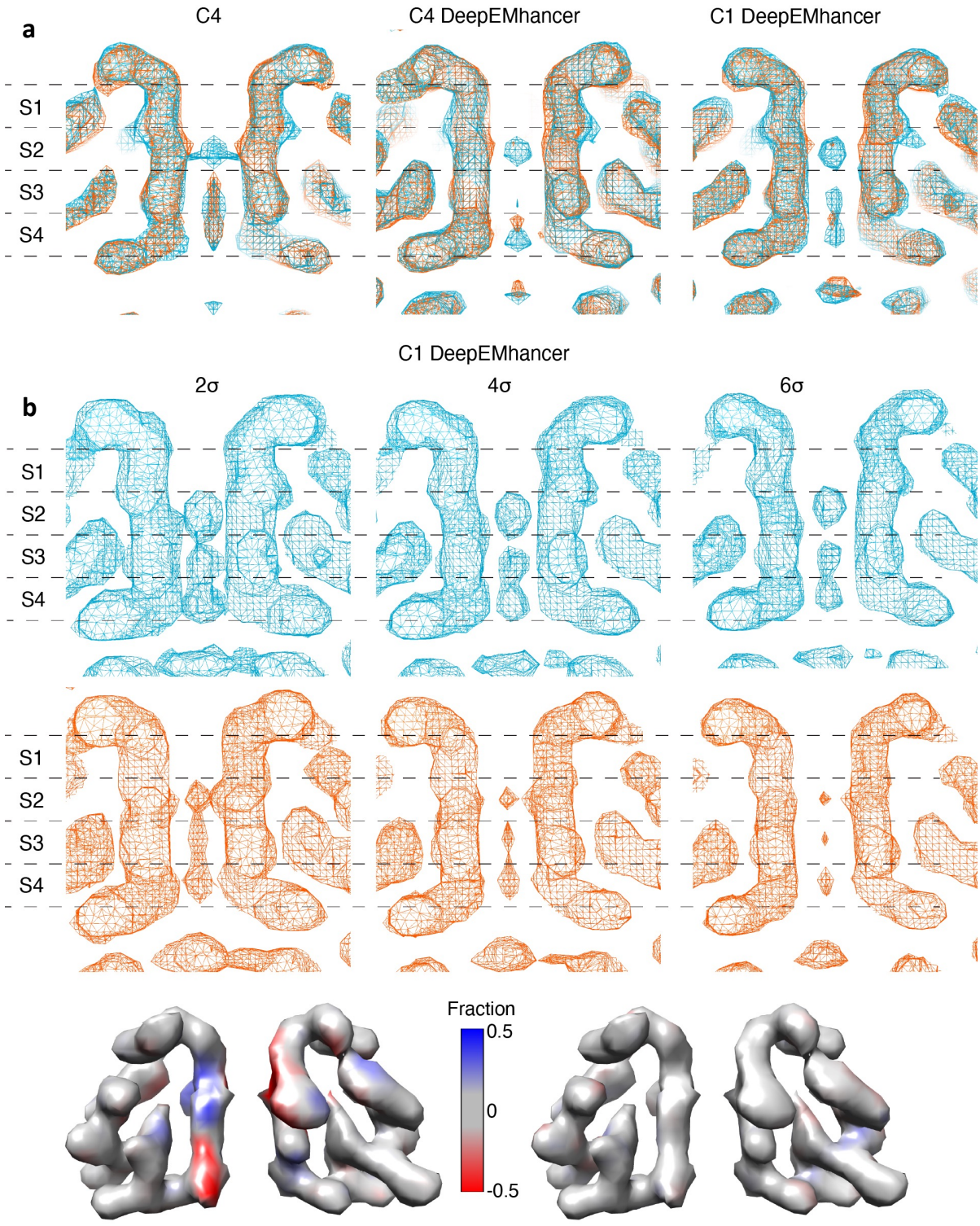

Supplementary Figure 3: Comparison of cryo-EM map inside the selectivity filter.
See over page for Figure Legend

Supplementary Figure 3

Supplementary Figure 3: Comparison of cryo-EM maps inside the selectivity filter.

a. Cryo-EM maps of high-K (blue) and low-K (orange) reconstructed with different post-processing methods: Reconstructions with C4 symmetry imposed and post-processed using (i) RELION[37] and (ii) DeepEMhancer[39], (iii) Reconstruction with no symmetry imposed and post-processed using DeepEMhancer[39]. **b.** Reconstruction with no symmetry imposed and post-processed using DeepEMhancer[39] at different sigma level. Clear Coulomb densities can be seen in high-K maps at ion coordination sites (S2/S3/S4). **c.** Fractional difference in density between maps with colour code depicting relative difference in densities for (i) high-K and low-K C4 reconstructions highlighting movement of selectivity filter and (ii) low-K reconstructions with and without C4 symmetry imposed.

Supplementary Figure 4

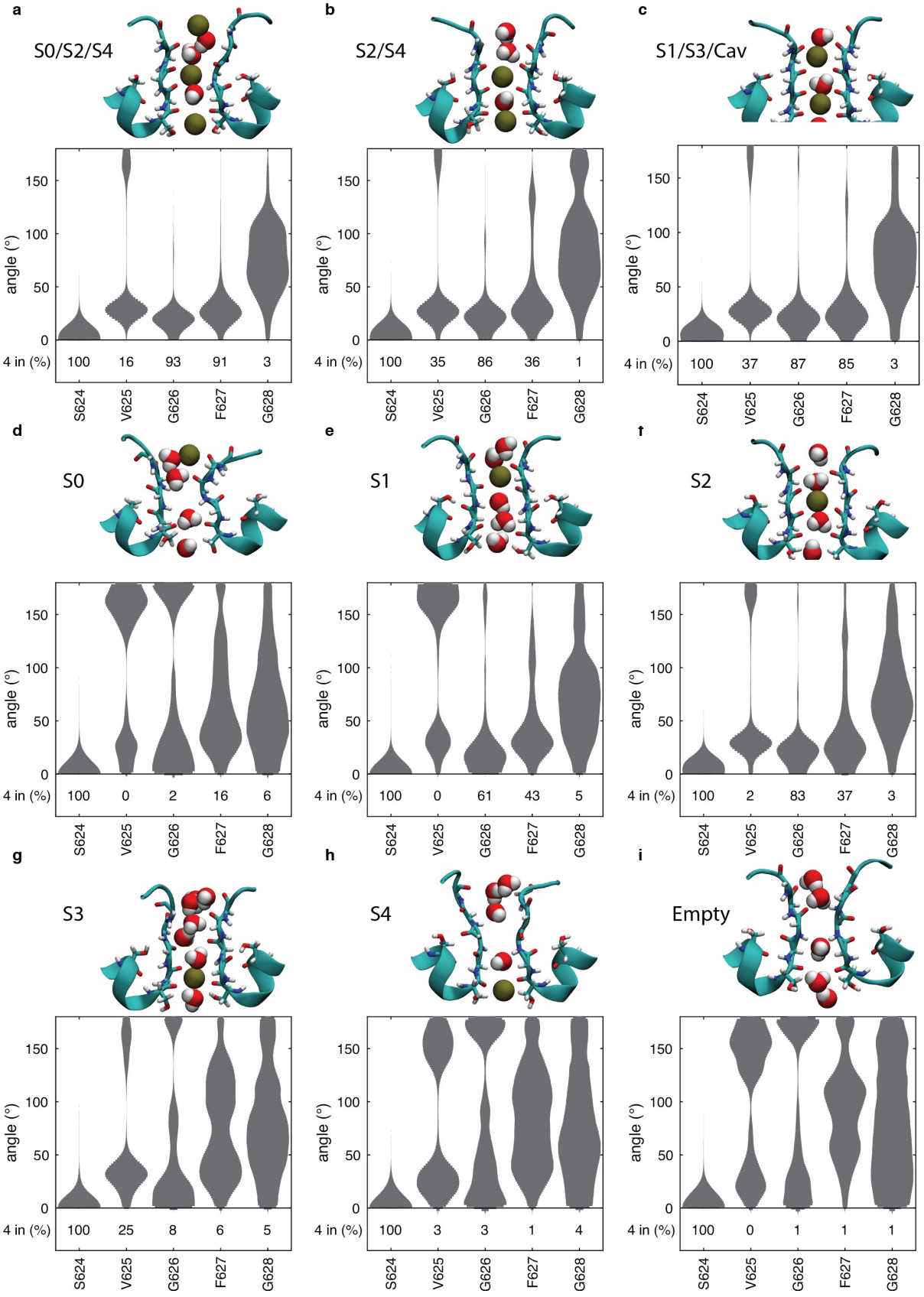

Supplementary Figure 4: MD simulations to explore the effect of K^+ ions on selectivity filter conformation.

(see over page for legend)

Supplementary Figure 4 continued

Supplementary Figure 4: MD simulations to explore the effect of K^+ ions on selectivity filter conformation. Distribution plots of the angle of the backbone carbonyls in the selectivity filter (defined as the absolute value of the angle between the vector made up by Cα and the carbonyl oxygen atom and Cα and the centre of mass of the selectivity filter) (top) and the frequency of four carbonyls pointing in (with an angle of < 70 degrees) (bottom) for ions held in **a.** S0/S2/S4, **b.** S1/S3/Cav, **c.** S2/S4, **d.** S0, **e.** S1, **f.** S2, **g.** S3, **h.** S4, and **i.** an empty selectivity filter. Insets in each panel show typical ion configurations. When K^+ ions were maintained in S0/S2/S4, S2/S4 or S1/S3/Cav (a-c), there were periods of time when Val625 carbonyls were seen to flip to no longer be directed into the pore, with all four carbonyls pointing towards the channel axis only 16%, 35% and 37% of the time. However, when the filter was empty (i), there were never four Val625 carbonyls pointing towards the channel axis. When an ion was placed in S0, S1 or S4 (d, e, h), the selectivity filter resembles that of the empty filter, with two or more carbonyls flipped 95%, 99% and 56% of the time, respectively, shown by a larger density of big angles in the probability similar to that of an empty selectivity filter (i). When an ion was placed in S2 or S3 (f and g), the selectivity filter resembles that of a filter with a multiple-ion configuration (carbonyls mostly directed inward with three or more carbonyls pointing in 94% and 80% of the time) (a-c). Even with an ion held in S2, we still observed that Val625 can flip, with one or two flipping 91% and 6% of the time, respectively.

Supplementary Figure 5

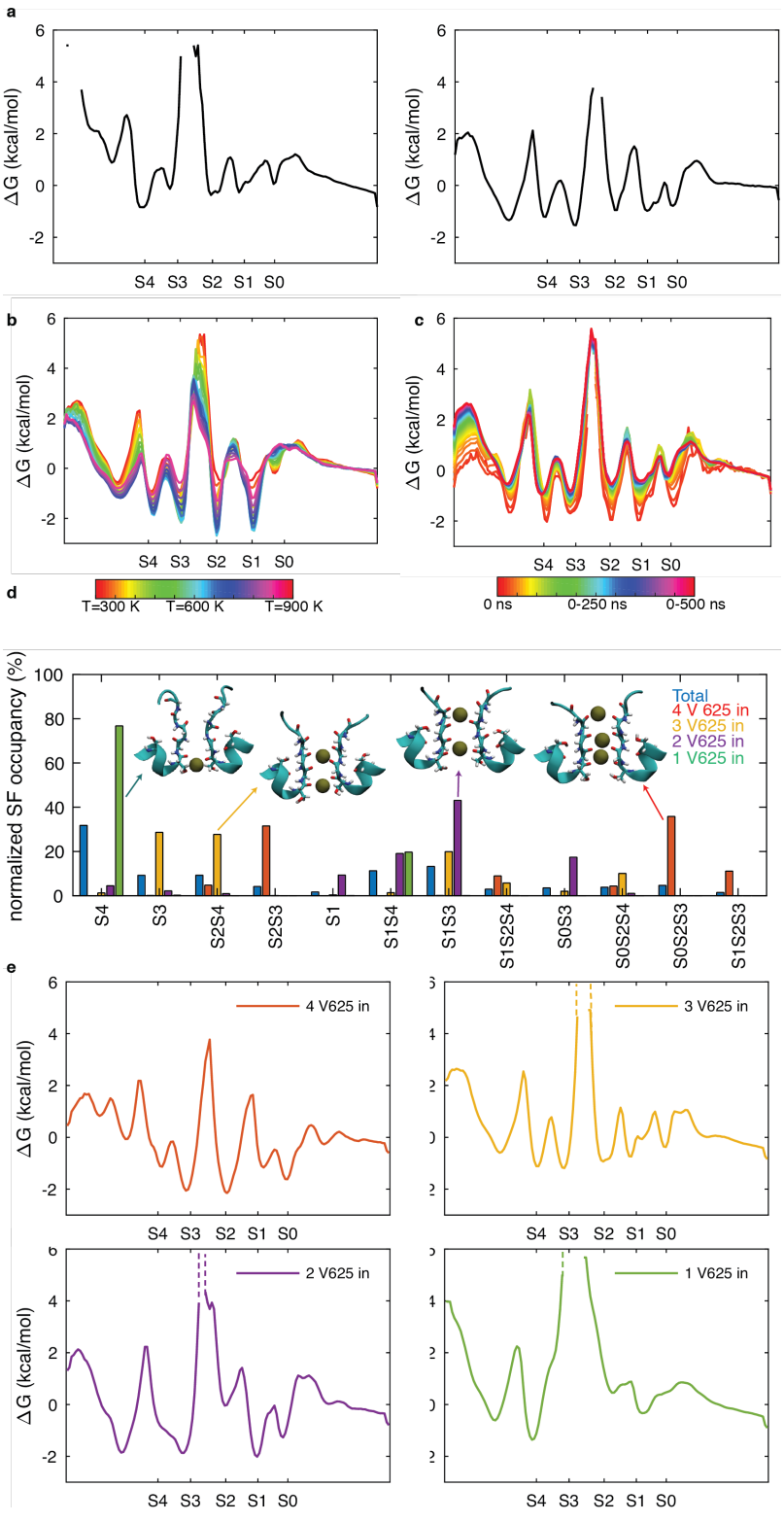

Supplementary Figure 5. REST2 simulations.

(see over page for Legend)

Supplementary Figure 5 continued

a. Free energy profiles for REST2 simulations[22] with ions starting in S0/S2/S4 (left) and S1/S3/Cav (right). **b.** Free energy profile for all 16 replicas with temperatures varying from 300 K to 900 K. The higher temperature replicas show shallower minima and lower barriers with a well captured barrier between S2 and S3. **c.** Convergence of the free energy of ions in the selectivity filter show how the free energy profile converges to within 1 kcal/mol in the selectivity filter in 70 ns. **d-e.** Throughout the REST2 simulations, we observed extensive fluctuations in the selectivity filter, with frequent flipping and unflipping of Val625 carbonyls. When all four Val625 carbonyls were directed inward (13 % of the time; shown in red), there was on average 2.7 ions in the selectivity filter, most commonly with ions in S2/S3, S0/S2/S3 or S1/S2/S3 suggesting that there is ion pairing in sites S2 (d; red). The free energy profile show deepest binding in S0, S2 and S3 with S1 and S4 elevated by 1 kcal/mol. There are small barriers for movement between S0-S1 and S3-S4 (~1 kcal/mol) with medium barriers for movement between S1-S2 and to exit the filter (~2-3 kcal/mol), and a large barrier that is too high to be captured for crossing between S2-S3 (e; red). More commonly, when three Val625 carbonyl oxygens were pointing in towards the channel axis (31% of the time; shown in yellow), there was an average of 1.9 ions in the selectivity filter maintaining good binding in all sites (d; yellow). In the free energy profile a displacement of the S3 ion downwards can be seen and S1 and S2 are not well defined, instead the free energy profile shows multiple minima in this area (e; yellow). These arise when the Tyr627 and Gly628 carbonyls flip and the selectivity filter widens, which creates off axis binding where the ion interacts with four carbonyl oxygens from two neighbouring residues and subunits. When two carbonyls were pointing inwards (16% of the time, almost exclusively in neighbouring subunits; shown in purple) there was, on average, 2.0 ions in the selectivity filter, most commonly occupying S3 as well as S1 or S2 (d; purple). S3 and S4 have now merged into one site which is positioned around the Ser624 carbonyl plane (e; purple). Noticeably, there is reduced binding in the S2 site that may be expected to inhibit conduction. 39% of the time a single carbonyl oxygen was pointing in towards the channel axis (shown in green), with an average ion occupancy of 1.5. Now the ions almost exclusively bind to S4 and on the Gly626 carbonyl oxygen plane between S0 and S1, vacating the entire centre of the selectivity filter and prohibiting ion translocation (d; green). It was very unlikely (0.0052% of the time) that all Val625 carbonyls were flipped outward (not shown).

Supplementary Figure 6

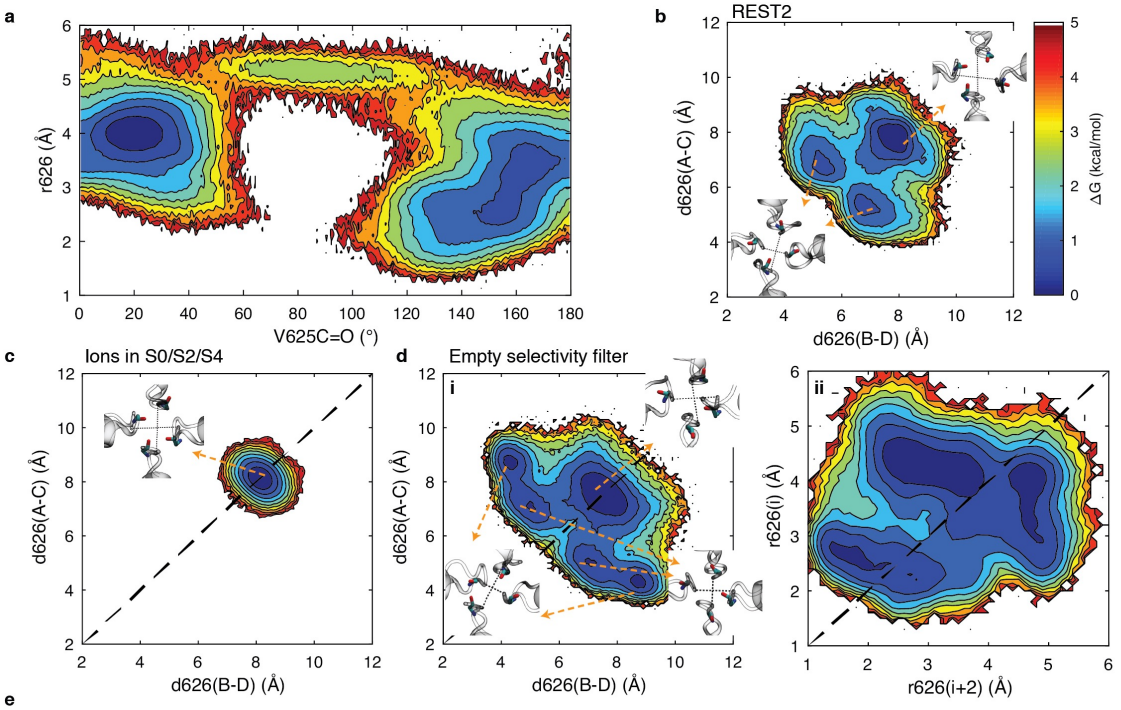

e

	Cluster occupancy (%)							
Cluster	Conductive-like	Inactivated-like	Flipped G626	Flipped F627	Flipped V625 and G626	Flipped F627	Flipped G626, F627 and G628	Flipped G628
total	41	30	4.8	4.8	4.7	4.7	4.2	3.6
S0/S2/S4	73	22	0	0.61	0.025	0.062	0	3.8
S2/S4	64	17	0	1.1	0.055	8.9	0	8.2
S1/S3/Cav	71	17	2.4	2.2	0.33	1.4	0.14	5.7
S0	11	41	9.8	9.7	16	2.9	4	1.7
S1	25	53	4.4	8.3	3.8	3.7	0.73	1.2
S2	57	25	2.5	4.2	0.34	4.1	0.20	4.2
S3	45	21	6.1	2.9	0.054	10	6.3	4.0
S4	19	33	13	7.1	5.5	8.2	12	0.14
Empty	7.5	39	5.5	7.2	16	2.5	14	3

f

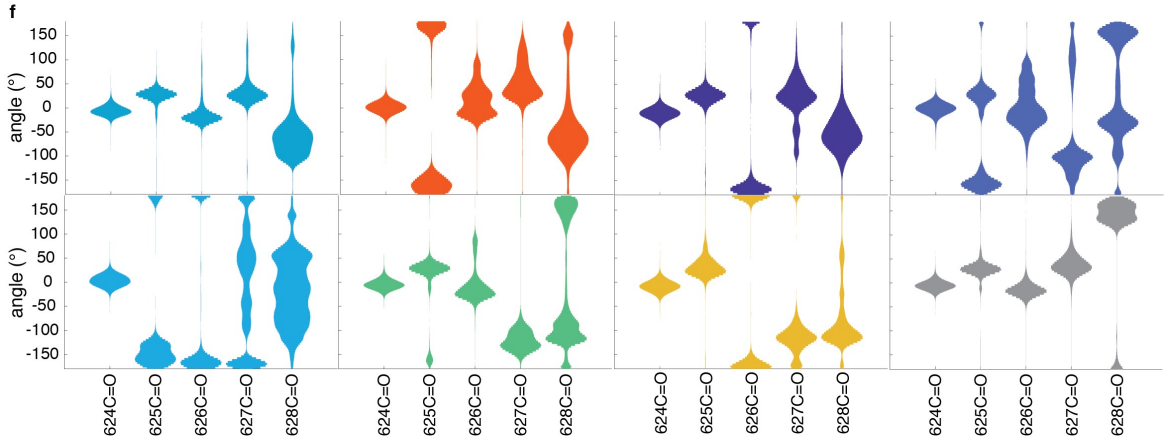

Supplementary Figure 6. MD simulations with different K^+ ion conformations clustered according to backbone dihedral angles of each subunit of the selectivity filter.

Supplementary Figure 6

a. 2-dimensional free energy maps highlighting the relationship between the flipping of the Val625 carbonyl (define angle) and the pinching of the Gly626 (represented as a mean radial position of Gly626 Cα atoms, r626) . **b-d.** 2-dimensional free energy maps showing the pinching of Gly626 Cα based on the distance between opposing subunits in: REST2 simulations (**b**); MD simulations with ions constrained in S0/S2/S4; and (**c**) and for an empty selectivity filter **(di**). **dii.** 2-dimensional free energy map showing the relationship between the radial positions of Gly626 Cα in two opposing subunits during the pinching of Gly626. Although **di** suggests an asymmetric collapse with 2-fold symmetry, it is apparent from **dii** that this arises predominantly due to movements only in one of the two subunits, which is in contrast to the C2 symmetrical inactivated state suggested by Li and colleagues[23] . **e.** Table showing the occupancy (rows) for the 8 major clusters obtained from analysis of Selectivity Filter backbone atoms across all MD simulations (columns). The occupancy in each cluster across all simulations is shown on row 3 and for each ion-configuration simulation on rows 4-12. There were two clusters; one in a conductive-like state with the Val625 carbonyl pointing towards the channel axis (41% total occupancy) and one in an inactivated-like state with the Val625 carbonyl pointing out with a narrowing at G626 (30% total occupancy). Analysis of these two clusters are shown in Figure 3 in the main manuscript. The additional 6 clusters, which had various backbone residues flipped, had occupancies between 3% and 5. When ions were placed in S0/S2/S4, S2/S4, S1/S3 or S2, the subunit maintained a conductive conformation the majority of the time (a; second column). This suggests that there has to be multiple ions in the selectivity filter (including S2 or S3), or S2 has to be occupied, for the selectivity filter to be conductive. **f.** Distribution plots of the angle of the backbone carbonyls in the selectivity filter for the 8 most commonly observed clusters.

Supplementary figure 7

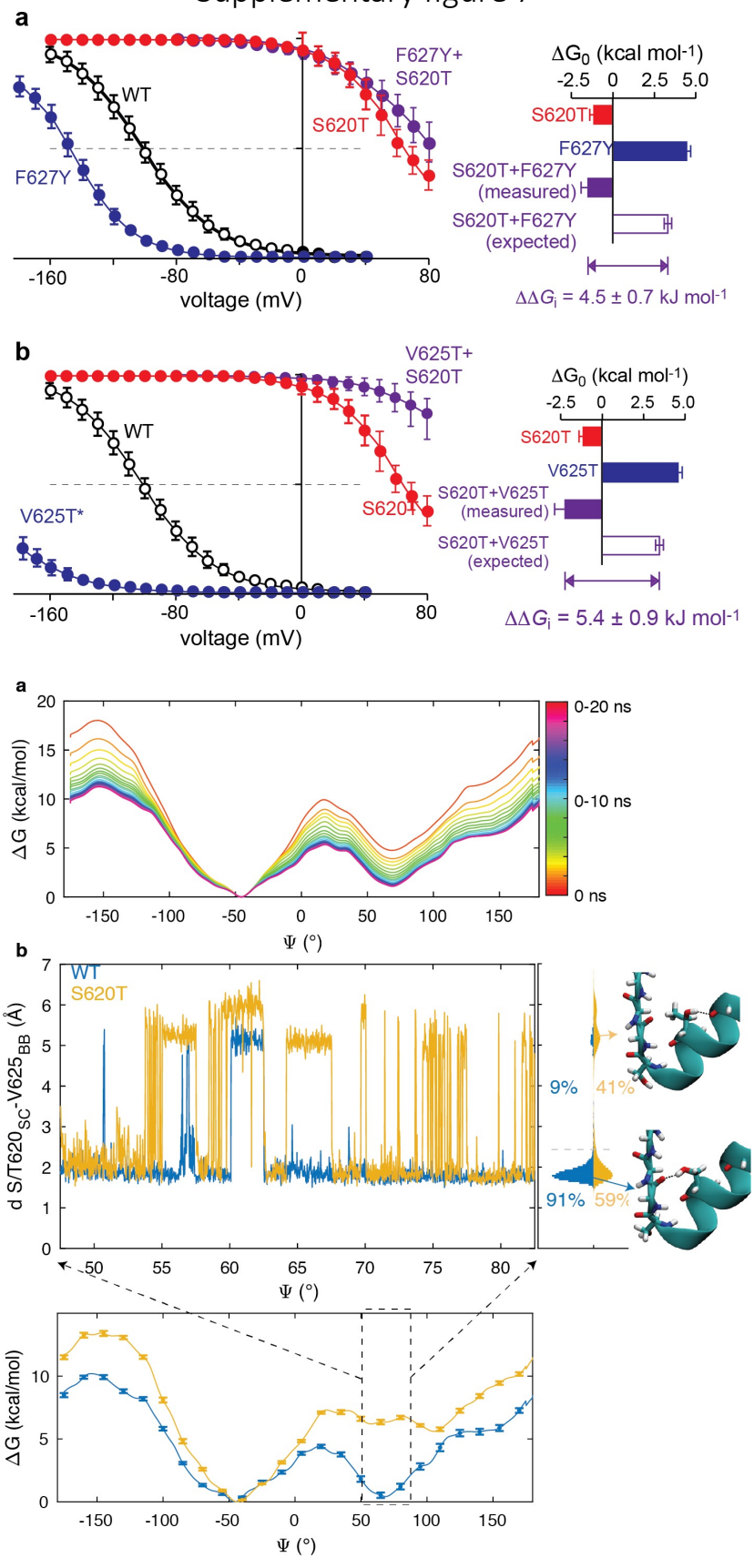

Supplementary Figure 7: Impact of S620T on inactivation of HERG channels

(legend continued over page)

Supplementary Figure 7: Impact of S620T on inactivation of HERG channels

Summary of the effect of **a.** S620T, F627Y and the combination S620T-F627Y mutant and **b.** S620T, V625T and the combination S620T-V625T on inactivation of HERG. Data points are shown as mean ± SEM. Curves represent best fits of a Boltzmann function to the data[33]. The panels to the right summarizes the ΔG_0 values for the mutants as well as the expected value for the combo mutants, i.e. if the two mutants do not interact then the effect of each mutant should be additive. The difference between the expected additive effect and the measured effect of the combo mutants reflects the interaction energy.

* Currents for V625T had to be measured in 100 mM KCl, to see any inactivation. It is therefore likely that we have underestimated the perturbation this mutant causes to inactivation and also underestimated the potential interaction energy between V625T and S620T.

We also tested Tyr616 mutants but were not able to get sufficient expression (Y616A) or if expressing able to accurately determine steady state inactivation (Y616I), similar to previous reports[10,61].

c. Umbrella sampling[58] of rotation of the Ψ-angle of the Val625-Gly626 linkage with ions held in the S0/S2/S4 configuration. **a.** Convergence plot for the free energy profile for WT channel with ions in S0/S2/S4 (the convergence plots for other ion occupancies, mutations and with voltage have similar behaviour (not shown)). **b.** The distance between the Ser/Thr620 sidechain hydroxyl and the Val625 backbone carboxylate at the location of the inactivated minimum (Val625 Ψ angles between 50° and 80°) for wild type hERG (blue) and S620T (orange). The violin plot to the right summarize the distribution of angles. Cartoons highlight how the Ser620 sidechain interacts with Val625 backbone 91% of the time (bottom) whereas in Thr620 this interaction is not present 59 % of the time (top).

Supplementary figure 8

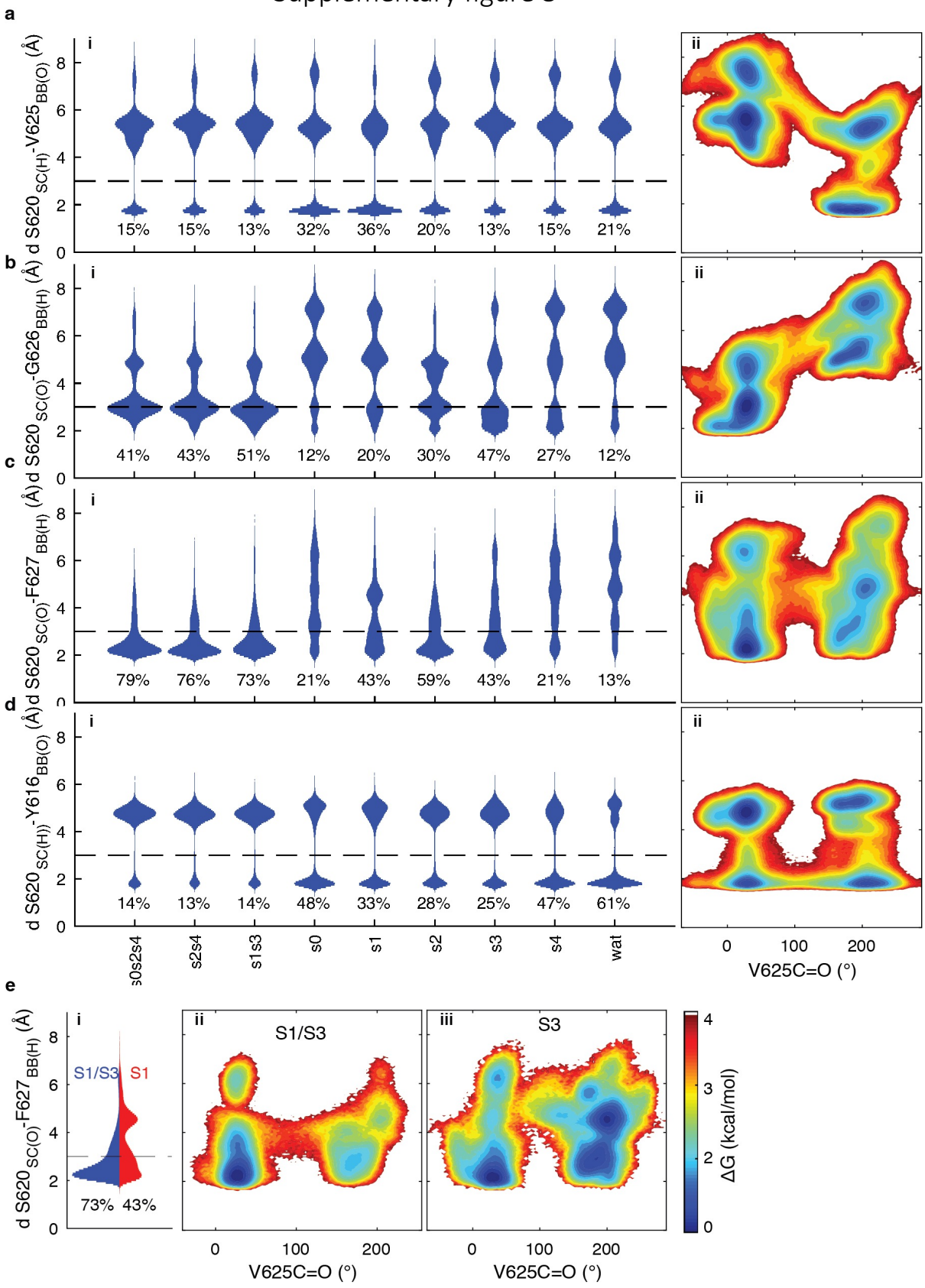

Supplementary Figure 8. Interactions behind the selectivity filter for MD simulations with different K^+ ion conformations.

(Legend continued on next page)

Supplementary figure 8

Supplementary Figure 8. Interactions behind the selectivity filter for MD simulations with different K^+ ion conformations.

a-d. Distribution plots for the distance between the Ser620 sidechain hydroxyl and (a) Val625 C=O, (b) Gly626 N-H, (c) Phe627 NH and (d) Tyr616 C=O as a function of ion occupancy of the filter (i) and 2-dimensional free energy plots as a function of rotation of the Val625 carbonyl (ii). **e.** Distribution plot (i) and 2-dimensional free energy plots (ii,iii) highlighting the difference in the interaction between the Ser620 sidechain and the Phe627 amide between channels with ions in S1/S3 and S3. As the ion leaves the top of the selectivity filter the Ser620-Phe627 interaction is less prevalent.

Supplementary Figure 9

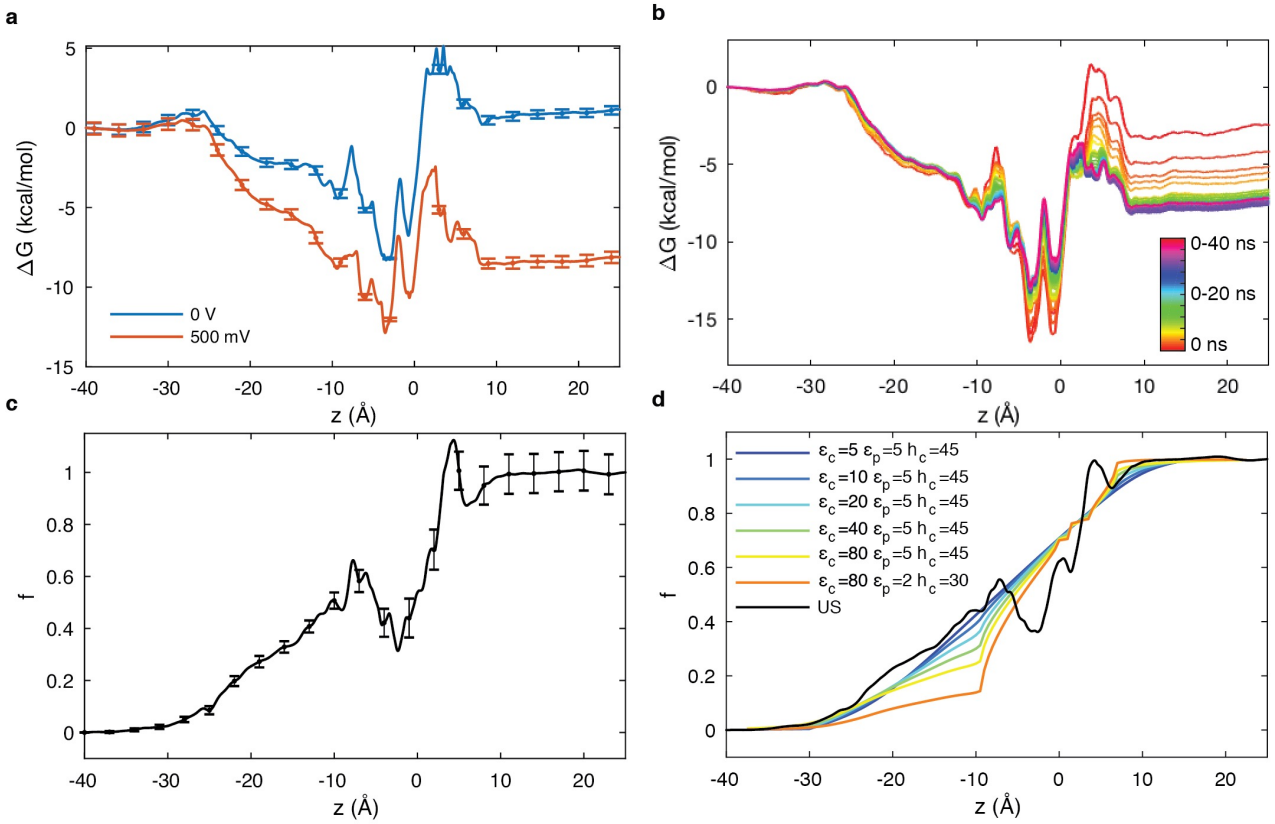

Supplementary Figure 9. Electric Field across the pore of hERG channels

a. The free energy profile for a single K^+ ion passing though the pore of a conductive hERG channel with 0 mV (blue) and 500 mV (red) membrane potential. **b.** Convergence of free energy profile for a single K+ ion passing though the pore of a conductive hERG channel with 500 mV membrane potential. **c.** The fraction of the field felt by a K^+ ion as it passes though the hERG pore from umbrella sampling. **d.** The fraction of the field felt by the K^+ ion as it passes though the hERG pore from US (black line) and based on calculations from the Poisson Boltzman equation[60] with different parameters ($5<\varepsilon_{cylinder}<80$,$2<\varepsilon_{protein}<5$ and $30<h_{cylinder}<45$ Å) (coloured lines).

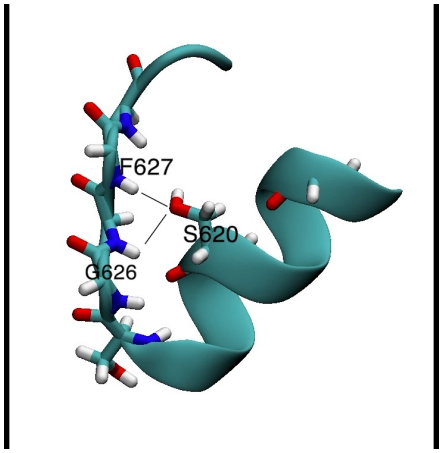

Supplementary Movie 1. Interactions between Ser620 and the selectivity filter

Movie showing how the Ser620 sidechain can interact with the backbone of Gly626 and Phe627 (H) or the backbone of Tyr616 (O) in the conductive state (Figure **5a,b**). When the sidechain of Ser620 interacts with the backbone of Tyr616 (O) (Figure **5c,d**), the Val625 carbonyl can flip outward (Figure **5d,e**). The sidechain of Ser620 can then interact with the backbone of Val625 (O) (Figure **5e**) or the backbone of Tyr616 (O) (Figure **5d**) in the inactivated state.